Inorganic Chemistry

ARTICLE

pubs.acs.org/IC

Photoluminescent Copper(I) Complexes with Amido-Triazolato Ligands

Gerald F. Manbeck, William W. Brennessel, and Richard Eisenberg*

Department of Chemistry, University of Rochester, Rochester, New York 14627, United States

Supporting Information

ABSTRACT:

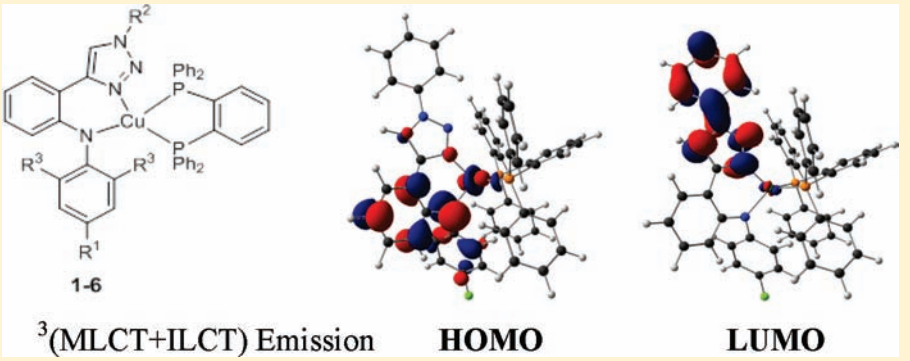

A series of heteroleptic copper(I) complexes incorporating amido-triazole and diphosphine ligands, [Cu^{I}(*N*-phenyl-2-(1-phenyl-1*H*-1,2,3-triazol-4-yl)aniline)(dppb)] (**1**), [Cu^{I}(*N*-(4-methylphenyl)-2-(1-phenyl-1*H*-1,2,3-triazol-4-yl)aniline)(dppb)] (**2**), [Cu^{I}(*N*-(4-methoxyphenyl)-2-(1-phenyl-1*H*-1,2,3-triazol-4-yl)aniline)(dppb)] (**3**), [Cu^{I}(*N*-(4-chlorophenyl)-2-(1-phenyl-1*H*-1,2,3-triazol-4-yl)aniline)(dppb)] (**4**), [Cu^{I}(2,6-dimethyl-*N*-[2-(1-phenyl-1*H*-1,2,3-triazol-4-yl)phenyl]aniline)(dppb)] (**5**), [Cu^{I}(2,6-dimethyl-*N*-[2-(1-benzyl-1*H*-1,2,3-triazol-4-yl)phenyl]aniline)(dppb)] (**6**), (dppb = 1,2-bis(diphenylphosphino)benzene), have been prepared. The complexes adopt a distorted tetrahedral geometry in the solid state with the amido-triazole ligand forming a six-member ring with the Cu(I) ion. The complexes exhibit long-lived photoluminescence with colors ranging from yellow to red-orange in the solid state, in frozen glass at 77 K, and in fluid solution with modest quantum yields of up to 0.022. Electrochemically, complexes **1**−**4** show irreversible oxidation waves while **5** and **6** are characterized by quasi-reversible oxidations as determined by cyclic voltammetry. For **1**−**4**, the emission energy and oxidation potential are found to vary linearly with the Hammett parameter σ_p of the substituent in the *para* position of the amido ligand, while in **5** and **6**, large differences in emission are observed because of the nature of N3 substitution in the triazole ring. Density functional theory calculations have been performed on the singlet ground states (S_o) of all complexes at the BP86/6-31G(d) level to assist in assignment of the excited states. On the basis of both experimental and computational results, we have assigned the excited states as intraligand + metal-to-ligand charge transfer ^{3}(ILCT+MLCT) or ligand-to-ligand charge transfer mixed with MLCT ^{3}(MLCT +LLCT) in these complexes.

INTRODUCTION

Organic light emitting diodes (OLEDs) are becoming the preeminent technology in flat panel displays because of their superior viewing quality, efficiency, and durability. OLEDs work on the principle of light emission upon charge recombination. Upon application of an external potential, electrons and holes migrate from the cathode and anode, respectively, to form light-emitting excitons at a luminescent compound. Since spin statistics dictate that 75% of the excitons are triplet states, heavy metal dopant emitters are desirable because they induce rapid inter-system crossing and triplet emission, thereby enhancing device efficiency.[1] Conversely, for organic emitters, only singlet excitons lead to emission while the triplet excitons are wasted. For device fabrication, spin coating and vapor deposition methods are used although the latter is generally preferred. This preference imposes a constraint that ideal dopants should be thermally stable and sublimable.

While iridium(III) and platinum(II) complexes have found extensive application in OLED's, there is also considerable interest in the use of luminescent copper(I) complexes as dopant emitters.[2−11] Although luminescence in Cu(I) complexes is well-known, many of these complexes suffer from poor emission efficiency or are cationic and thus unsuitable for device fabrication by vapor deposition methods. One notable exception is a di-nuclear complex reported by Peters and co-workers in 2005. The complex, which is supported by a PNP ligand set exhibited an unusually high quantum yield and long-lived excited state.[12] It was

Received: November 22, 2010
Published: March 21, 2011

Chart 1. 1,2,3-Triazole Ligands and Relevant Copper Complexes[a]

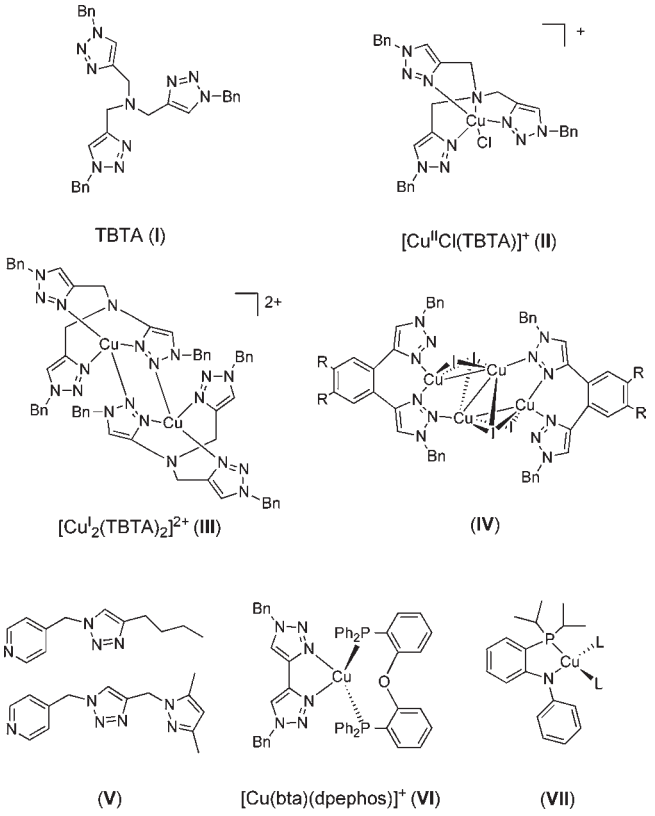

[a](**I**) Ref 35. (**II, III**) Ref 36. (**IV**) Ref 39. (**V**) Ligands used in ref 40. (**VI**) Ref 41. (**VII**) Ref 43.

also thermally stable and has been incorporated in an OLED device with a 16% external quantum efficiency.[13,14]

The performance of Peters' neutral complex in a device has stimulated the synthesis of other new copper(I) complexes exhibiting the properties desirable for device performance and fabrication, specifically sublimability, thermal stability, and bright photoluminescence. While modification of commonly used ligands such as phenanthroline or bipyridine represents a reasonable approach for the development of new complexes, a second option involves the use of previously unemployed ligands.

One underutilized ligand set is composed of chelating agents containing 1,4-disubstituted-1,2,3-triazoles that are readily made via Cu(I)-catalyzed Huisgen dipolar cycloaddition.[15−17] Due in part to the simplicity of synthesis as well as the broad potential for variation in design, numerous reports on the coordination chemistry of triazoles and chelating ligands containing them have appeared recently in the literature.[18−34] Among these reports are a number of new copper(I) triazolato complexes. In 2004, tris-(benzyltriazolylmethyl)amine (TBTA) (**I**) was used as an effective ligand for Cu(I) in cycloaddition reactions, presumably stabilizing the catalyst through chelation.[35] Later, evidence regarding the coordination modes of this ligand was obtained through structural characterization of $[Cu^{II}Cl(TBTA)]^+$ (**II**) and an air-sensitive dinuclear complex, $[Cu^{I}_2(TBTA)_2]^{2+}$ (**III**).[36] A related complex, [Cu^ICl(tris(triazolyl)methanol)], was prepared as an air-stable complex that exhibited high catalytic activity, but its structure was inferred indirectly.[37] A polymer-supported Cu(I)

Scheme 1[a]

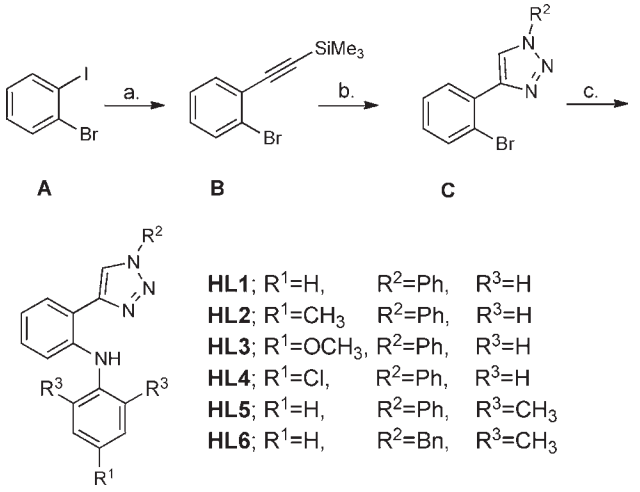

[a] Conditions: (a) $PdCl_2(PPh_3)_2$ (1%), CuI (3.5%), trimethylsilyl-acetylene, iPr_2NH, 25 °C, 6 h. (b) K_2CO_3, phenyl azide or benzylbromide/NaN_3, sodium ascorbate (6−10%), $CuSO_4$ (3−5%, 0.5 M in H_2O), *t*-BuOH/H_2O 1:1, 60 °C, 12 h. (c) $Pd(OAc)_2$ (5%), dppf (7.5%), NaOtBu (1.3 equiv), Ar(−2,6-R^3-4-R^1)NH_2, toluene, 100 °C, 48 h.

species coordinated by triazole and pyridyl groups has been described for biphasic catalysis.[38]

Photophysical properties of Cu(I) complexes with 1,2,3-triazole ligands (Chart 1) have been examined by us[39] and others[40−42] (**IV**−**V**). Depending on the organic ligand, cuprous iodide complexes containing triazoles with pendant pyridyl or pyrazole groups (**V**) form luminescent polymeric metal organic frameworks.[40] We have recently shown that symmetric chelating triazoles linked by a phenylene backbone react with CuI in a 1:2 ratio to provide discrete tetranuclear clusters which are brightly luminescent in the solid state (**IV**).[39] However, the high molecular weight of these compounds rendered them unsuitable for sublimation and vapor deposition processing. Encouraged by the bright emission, we hypothesized that neutral mononuclear complexes with amido-triazole and diphosphine chelating ligands may exhibit similar bright luminescence and thermal stability. Related work on mononuclear Cu(I) complexes with amido-phosphine supporting ligands (**VII**) has in fact led to complexes with highly efficient solution photoluminescence.[43] Herein, we report the synthesis and photophysical properties of neutral, mononuclear copper(I) complexes supported by chelating amido-triazole ligands and 1,2-bis(diphenylphosphino)benzene (dppb).

RESULTS AND DISCUSSION

Synthesis of the Ligands. Ligand precursors **HL1**−**HL6** were prepared in three steps as outlined in Scheme 1. Briefly, the Sonogoshira coupling reaction of commercially available 1-bromo-2-iodobenzene (**A**) with trimethylsilyl acetylene provided compound **B**. TMS-protected **B** was then subjected to one-pot deprotection and Cu(I)-catalyzed Huisgen cycloaddition with phenyl azide or benzyl azide generated in situ from benzyl bromide and NaN_3. This convenient single pot sequence has been used before by us[39] and others.[30] Finally, aryl amination of **C** using $Pd(OAc)_2$/dppf as the catalyst[44] proceeded in good yield to provide the ligand precursors **HL1**−**HL6** after

dx.doi.org/10.1021/ic102338g |*Inorg. Chem.* 2011, 50, 3431–3441

chromatographic purification. The ligand precursors were characterized by mass spectrometry and ^{13}C and ^{1}H NMR spectroscopy. For **HL1**−**HL4**, the NH proton resonance in $CDCl_3$ was broadened into the baseline. In **HL5** and **HL6**, the NH resonance appeared significantly downfield at 8.86 and 8.94 ppm respectively. The observed chemical shift was interpreted as an effect of hydrogen bonding with the triazole ring that was later confirmed by an X-ray structure analysis of **HL5**.

Synthesis of the Complexes and X-ray Crystallography. Complexes **1**−**6** were prepared by treating a tetrahydrofuran (THF) slurry of $Cu_2(\mu_2\text{-}Cl)_2(dppb)_2$ (dppb = 1,2-bis-(diphenylphosphino)benzene) with a mixture of potassium *tert*-butoxide and the ligand precursor in THF. During the addition, a rapid color change from yellow to orange occurs with concurrent dissolution of the $Cu_2(\mu_2\text{-}Cl)_2(dppb)_2$ suspension. Gentle heating (5 min at 40 °C) is required for full consumption of the starting material. After removal of KCl by filtration, the desired compounds are precipitated with hexanes as yellow or orange solids. The complexes are highly soluble in THF, marginally soluble in benzene and ether, virtually insoluble in hexanes, and unstable in chlorinated solvents. The complexes oxidize slowly when exposed to air in the solid state, but decompose rapidly when exposed to oxygen in solution. ^{1}H NMR spectra recorded in C_6D_6 show characteristic amido-triazole ligand resonances which in many cases overlap with aromatic signals from the dppb ligand while ^{31}P NMR spectra exhibit a broad singlet for each complex. Parent ions with the correct isotope patterns were seen by mass spectrometry under atmospheric pressure ionization (APCI), and all complexes provided satisfactory combustion analyses.

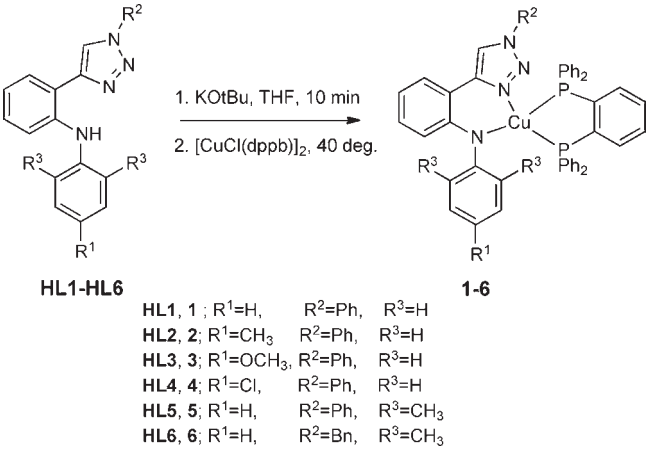

Single crystals of complexes **4**−**6** were grown from THF/hexanes mixtures. Additionally, the structure of **HL5** was solved for comparison of the free and coordinated ligand geometries. Unit cell, data collection, and structure refinement details are provided in Table 1, and selected bond lengths and angles are shown in Table 2. Full metrical parameters are provided in the Supporting Information as a cif file. Figure 1 is a perspective view of complex **5**. ORTEP diagrams of **4**, **6**, and **HL5** are shown in the Supporting Information, Figures S1−S4.

Complexes **4**−**6** each adopt a distorted tetrahedral geometry around the Cu(I) center as judged by the bond angles at the metal and the dihedral angles between planes containing chelating ligand donor atoms and copper(I) ions (Table 2). Regarding the latter, angles between chelating atoms (P2−Cu1−P1) and (N1−Cu1−N4) are near 90°, while

Table 1. Summary of Crystallographic Data

	4·1/4 THF	5	6·2 THF	HL5
formula	$C_{51}H_{40}CuN_4O_{0.25}P_2$	$C_{52}H_{43}CuN_4P_2$	$C_{61}H_{61}CuN_4O_2P_2$	$C_{22}H_{20}N_4$
fw	873.80	849.38	1007.62	340.42
T (K)	100.0(1)	100.0(1)	100.0(1)	100.0(1)
cryst syst	triclinic	triclinic	triclinic	monoclinic
space group	$P\bar{1}$	$P\bar{1}$	$P\bar{1}$	$P2_1/c$
a (Å)	13.006(4)	10.7576(9)	11.252(3)	8.8824(9)
b (Å)	16.949(6	11.0452(9)	13.518(3)	13.883(1)
c (Å)	19.756(8)	20.440(2)	16.918(4)	14.824(2)
α (deg)	87.334(8)	80.040(2)	82.476(4)	90
β (deg)	70.893(6)	79.368(2)	79.651(4)	100.077(2)
γ (deg)	82.130(6)	60.986(1)	86.882(4)	90
V (Å^3)	4076(2)	2077.5(3)	2508(1)	1799.7(3)
Z	4	2	2	4
ρ_{calcd} (g cm^{-3})	1.424	1.358	1.334	1.256
μ (mm^{-1})	0.724	0.645	0.549	0.076
no. reflns collected	44205	48129	19070	43136
no. unique reflns	14414	19741	8801	9575
R_{int}[a]	0.2963	0.0389	0.0983	0.0356
no. of obsd reflns	5353	14440	4900	7235
no. of params	1078	534	633	315
GOF[b] on F^2	0.930	1.021	0.970	1.027
R1 [$I > 2\sigma(I)$][c]	0.0856	0.0423	0.0512	0.0514
wR2[d]	0.1162	0.1027	0.0812	0.1350

[a] $R_{int} = |F_o^2 - \langle F_o^2 \rangle|/|F_o^2|$. [b] GOF = $S = [\Sigma[w(F_o^2 - F_c^2)^2]/(m-n)]^{1/2}$, where m = number of reflections and n = number of parameters. [c] $R1 = \Sigma||F_o| - |F_c||/\Sigma|F_o|$. [d] $wR2 = [\Sigma w(F_o^2 - F_c^2)^2/\Sigma w(F_o^2)^2]^{1/2}$ where $w = 1/[2(F_o^2) + (aP)^2 + bP]$ and $P = 1/3 \max(0, F_o^2) + 2/3\, F_c^2$.

dx.doi.org/10.1021/ic102338g |*Inorg. Chem.* 2011, 50, 3431–3441

N−Cu−P bond angles are all greater than 109°. Six-membered amido-triazole chelate rings are nearly planar, but the 5-membered diphosphine chelate rings are slightly buckled. The geometry of uncoordinated **L5**, where hydrogen-bonding exists between the diaryl amine and N1 of the triazole ring, is nearly identical to that of the coordinated ligand in **5**. In the free ligand, as well as in **4**−**6**, the phenylene and triazole rings deviate slightly from planarity (~14°).

For N3-phenyl complexes **4** and **5**, the phenyl rings and triazole heterocycles are nearly coplanar. In contrast, 4-chloro or 2,6-dimethyl substituted aryl rings are twisted approximately 90° out of plane of the central phenylene ring in each complex. The Cu−N1 distances are comparable to those observed in copper(I) halide clusters with triazole ligands,[39] but Cu−N4 distances are somewhat shorter than those reported in similar mononuclear Cu(I) compounds with chelating amido ligands (2.086(1) Å).[43] However, the Cu−N4 distances observed here are significantly longer than in the two-coordinate anilido complex [Cu(IPr)(NHPh)] (IPr = 1,3-bis(2,6-diisopropylphenyl)imidazol-2-ylidene) (1.841(2) Å).[45] The similarity between the Cu−N1 and Cu−N4 bond lengths confirms the single bond character of the amido ligand as the filled Cu d orbitals and filled nitrogen π orbital preclude a π-bonding interaction.

Table 2. Selected Bond Lengths (Angstroms) and Angles (Degrees)

	4[a]	5	6
Cu1−N1 (Cu2−N5)	1.981(7), 2.003(7)	1.996(1)	2.031(3)
Cu1−N4 (Cu2−N8)	1.989(7), 1.978(7)	1.964(1)	1.981(3)
Cu1−P2 (Cu2−P4)	2.253(3), 2.271(3)	2.2618(4)	2.273(1)
Cu1−P1 (Cu2−P3)	2.269(3), 2.236(3)	2.2180(4)	2.276(1)
N1−Cu1−N4 (N5−Cu2−N8)	92.3(3), 92.7(3)	92.05(4)	93.2(1)
N1−Cu1−P2 (N5−Cu2−P4)	115.0(2), 105.3(2)	104.34(3)	109.8(1)
N4−Cu1−P2 (N8−Cu2−P4)	126.5(2), 123.0(2)	125.70(3)	128.9(1)
N1−Cu1−P1 (N5−Cu2−P3)	111.1(2), 120.2(2)	112.10(3)	109.1(1)
N4−Cu1−P1 (N8−Cu2−P3)	123.7(2), 125.2(2)	130.55(3)	130.9(1)
P2−Cu1−P1 (P3−Cu2−P4)	89.5(1), 91.2(1)	90.47(1)	84.51(4)
P1, P2, Cu1 and N1, N4, Cu1	89	87	89
(P3, P4, Cu2 and N5, N8, Cu2)	82		

[a] There are two independent molecules in the asymmetric unit of complex **4**. Measurements refer first to the molecule containing Cu1 and the second measurement as well as parenthetical atom labels refer to the molecule containing Cu2.

Absorption Spectroscopy. The electronic spectra of complexes **1**−**6** were recorded in benzene as shown in Figure 2 and in THF as given in the Supporting Information. In both benzene and THF, the spectra of **1**−**5** are similar with three prominent features: an intense band from 280 to 300 nm with a molar extinction coefficient (ε) in the range of 18,000−24,000 M^{-1} cm^{-1}, a strong band appearing as a shoulder ranging from 325 to 440 nm, and a broad, low energy band with maxima from 415 to 430 nm and ε of 4,000−10,000 M^{-1} cm^{-1}. Consistent with the pale yellow solution color at dilute concentrations, the low energy bands of each complex extend into the visible region of

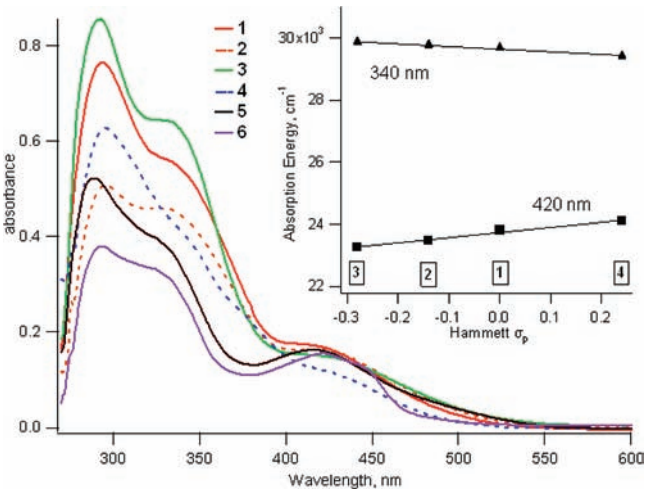

Figure 2. Absorption spectra for **1**−**6** in benzene ($c = 2.5 \times 10^{-5}$ M). Inset: Hammett plots of absorption energy versus σ_p of the substituent *para* to the amido donor (**1** = H, **2** = Me, **3** = OMe, **4** = Cl).

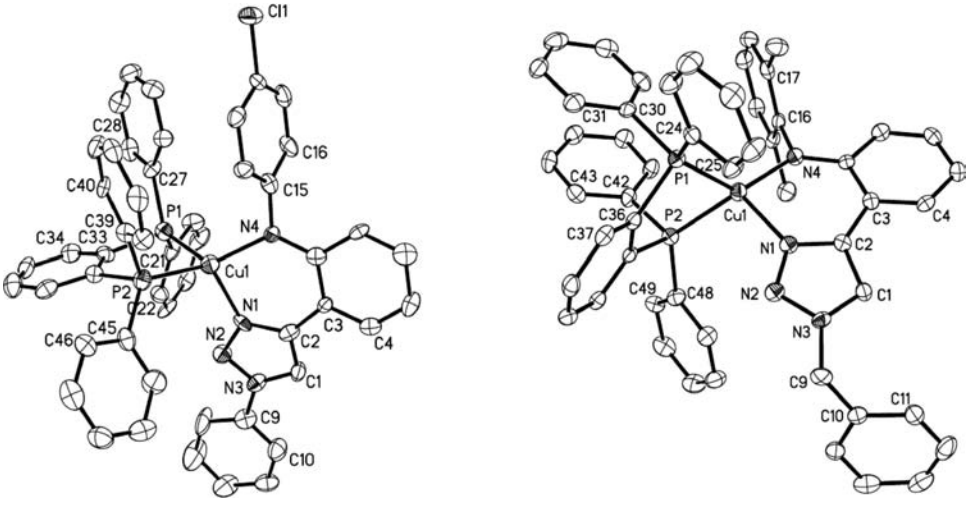

Figure 1. ORTEP diagrams of complex **4** (left) and complex **6** (right) (50% probability ellipsoids). Hydrogen atoms and cocrystallized solvent molecules have been omitted for clarity.

dx.doi.org/10.1021/ic102338g |*Inorg. Chem.* 2011, 50, 3431–3441

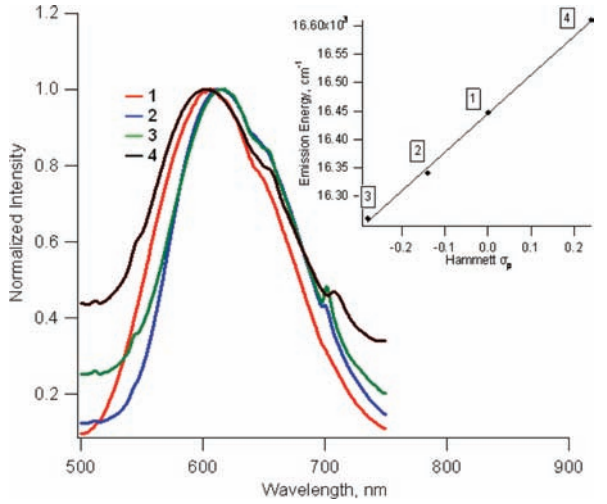

Figure 3. Solid state emission spectra for **1**−**4** at 298 K. λ_{exc} = 400 nm. Inset: Hammett plot of emission maximum versus σ_p values of the substituent *para* to the amido donor (**1** = H, **2** = Me, **3** = OMe, **4** = Cl).

the spectrum. The spectrum of complex **6** (Figure 2, solid purple line) is similar to those of **1**−**5** with the exception that the lowest energy band displays an additional feature with a maximum at 423 nm and a shoulder at 445 nm.

The energy of the strong absorption near 300 nm varies only slightly between complexes, suggesting little perturbation of the involved molecular orbitals by differences in the amide part of the anionic ligand. This band may be assigned as $\pi-\pi^*$ transitions of the numerous aromatic groups in the ligand set. The homoleptic cationic complex $Cu(dppb)_2^+$ exhibits a similar feature in its absorption spectrum.[46] On the other hand, the absorption energies of the bands near 340 and 420 nm vary noticeably between the complexes. In the series **1**−**4**, the maximum absorption wavelengths of both bands in benzene vary linearly with the Hammett σ_p constant of the substituent at the 4-position of the aryl amido group (Figure 2, inset). While the slope is negative for the shoulder near 340 nm, it is positive for the lower energy absorption. In THF, the data were not modeled as well by linear fits as in benzene, but the trends are similar (Supporting Information, Figures S5−S6). At the two extremes of the lower energy band in benzene, electron donating methoxy-substituted complex **3** exhibits the lowest energy maximum while electron withdrawing chloro-substituted **4** exhibits the highest energy maximum. This trend is consistent with increasing the highest occupied molecular orbital (HOMO) energy with greater electron donating properties of the substituent *para* to the amido donor. The absorption shoulder near 340 nm is affected in the opposite way, implying that electronic differences in the ligand influence the energy of the electron accepting orbital in this electronic transition.

Solid State and Frozen Glass Emission. Solid state emission spectra (Figure 3) were obtained for complexes **1**−**6** in KBr matrixes at 298 K and 77 K. Emission profiles are broad with maxima at 575−615 nm and shoulders for **1**−**5** in the 645−655 nm range (Table 3). Upon cooling to 77 K, only subtle changes in the emission maxima are observed (ca. 2 nm). Solid state emission decay curves were fitted to single exponential functions with lifetimes at 298 K ranging from 0.30 to 1.9 μs. At 77 K, there is a modest increase in the lifetime of **1**−**5** by about one order of magnitude.

In 2-methyl-tetrahydrofuran frozen glass at 77 K, the emission maxima are significantly blue-shifted from the solid state and lie in the range of 555−585 nm with lower energy shoulders evident in **1**−**5** (Table 3, Supporting Information, Figures S7−S8). Decay profiles in frozen glass samples were fit to single exponential functions with lifetimes ranging from 330 μs for **1** to 1400 μs for **5**.

The solid state emission of N-benzyl substituted complex **6** is blue-shifted relative to **1**−**5** at room temperature while the luminescence lifetime of 1.7 μs is similar to those of the other complexes. Upon cooling the solid state sample of **6** to 77 K, a red shift from 575 to 589 nm is observed. The excited state lifetime of **6** at 77 K in the solid state (270 μs) is considerably longer than that of the other complexes. In frozen 2-methyl-tetrahydrofuran, the emission at 567 nm is similar to **1**−**5**, with a lifetime of 70 microseconds that is notably shorter than those of **1**−**5**.

At 298 K, the solid state emission energy in **1**−**4** varies linearly with Hammett σ_p parameter of the aryl amido substituent (Supporting Information, Figure S12). The same trend (**4** > **1** > **2** > **3**) is observed in frozen glass samples (Supporting Information, Figure S9). Hammett plots of emission energy versus σ_p have a positive slope in which complex **3** with an electron-donating methoxy group exhibits the lowest energy emission. The same trend was found in the lowest energy absorption bands of these complexes and is consistent with electronic perturbation of the HOMO by the amido ligand substituent.

Complexes **1** and **5** both have H atoms in the R^1 position, yet the emission of **5** is red-shifted relative to that of **1** in the solid state and frozen glass by 16 and 10 nm, respectively. This observation may be explained in inductive electronic or stereoelectronic terms regarding the dimethyl substitution of **5**. Since the emission of **2** is red-shifted relative to **1** by 3−7 nm, a purely electronic argument suggests that a second methyl group might perturb the emission by a similar amount more. A stereoelectronic argument is that absence of free rotation around the N-aryl bond because of 2,6-dimethyl substitution results in electronic isolation of the aryl ring from the π system of the amide donor, the central phenylene ring, and the copper ion. Presumably, disrupted conjugation raises the energy of the involved molecular orbitals.

Comparison of the emission in complexes **5** and **6** provides some insight into the nature of the lowest unoccupied molecular orbital (LUMO). Complex **6** shows higher energy emission in frozen glass and in the solid state. Since absorption and emission data for complexes **1**−**4** have already established that substitution of the aryl ring in the amido part of the ligand affects the HOMO, the higher energy emission in **6** must arise from a higher triazole-based LUMO relative to **5** since the aryl amido part of the ligands are the same in both complexes.

Solution Emission. Emission spectra were measured in THF and benzene at room temperature. All complexes exhibit orange emission in fluid solution and relevant photophysical data are summarized in Table 3. When the complexes are excited in their lowest energy absorptions (420 nm), the emission profiles are broad with maxima ranging from about 630 to 660 nm and lower energy shoulders separated by about 25 nm from the maxima (Supporting Information, Figures S13−S24). For each complex, notably higher quantum yields were found in benzene than in THF with **4** exhibiting the highest emission quantum yield (Φ = 0.022) measured relative to $Ru(bpy)_3^{2+}$ in air-equilibrated water (Φ = 0.028).[47] The emission bands do not overlap with the absorption bands. With the exception of **3** and **6** in THF, lifetimes range from several hundred nanoseconds to a few microseconds,

Table 3. Summary of Photophysical Data

complex	media	absorptions λ/nm (ε/M^{-1} cm^{-1})>	λem/nm (τ /μs)[c]	Φ[d]
1	THF[a]	286 (31,680), 325 (24,800), 362 (18,480), 416 (9,480)	632, 658 (0.57)	0.0058
	benzene[a]	295 (24,200), 337 (31,000), 420 (9,800)	629, 651 (1.7)	0.016
	glass 77 K		567 (330)	
	solid 298 K		608 (1.9)	
	solid 77 K		610 (13)	
2	THF[a]	288 (23,360), 330 (17,600), 425 (6,810)	633, 662 (0.35)	0.0033
	benzene[a]	295 (23,800), 336 (18,700), 426 (6700)	632, 653 (1.0)	0.011
	glass 77 K		575 (310)	
	solid 298 K		612 (2.1)	
	solid 77 K		615 (6.1)	
3	THF[a]	287 (21,440), 328 (16,440), 436 (4,560)	633, 667 (0.07)	0.00040
	benzene[a]	296 (18,500), 335 (14,100), 430 (4,100)	634, 659 (0.20)	0.0019
	glass 77 K		583 (450)	
	solid 298 K		615 (0.59)	
	solid 77 K		613 (3.4)	
4	THF[a]	289 (20,640), 321 (15,640), 378 (15,640), 419 (5,160)	631, 649 (0.75)	0.010
	benzene[a]	298 (21,000), 340 (17,000), 415 (6,800)	622, 647 (2.4)	0.026
	glass 77 K		555 (490)	
	solid 298 K		602 (1.5)	
	solid 77 K		604 (11)	
5	THF[a]	284 (33,160), 330 (16,200), 416 (1,000)	631, 649 (2.0)	0.013
	benzene[a]	290 (27,000), 327 (17,000), 416 (8700)	628, 653 (2.8)	0.019
	glass 77 K		577 (1400)	
	solid 298 K		623 (0.30)	
	solid 77 K		626 (2.1)	
6	THF[a]	290 (22,320), 328 (11,720), 419 (8,400), 440 (6,480)	632, 658 (0.06)	0.0015
	benzene[a]	295 (18,500), 326 (13,400), 423 (7,000), 445 (5,600)	631, 653 (0.11)	0.0048
	glass 77 K		567 (70)	
	solid 298 K		575 (1.7)	
	solid 77 K		589 (270)	

[a] $c = 2.5 \times 10^{-5}$ M, (b) In 2-methyltetrahydrofuran (c) $\lambda_{exc} = 420$ nm. (d) Measured as a relative quantum yield using $Ru(bpy)_3^{2+}$ in water ($\Phi = 0.28$).[47]

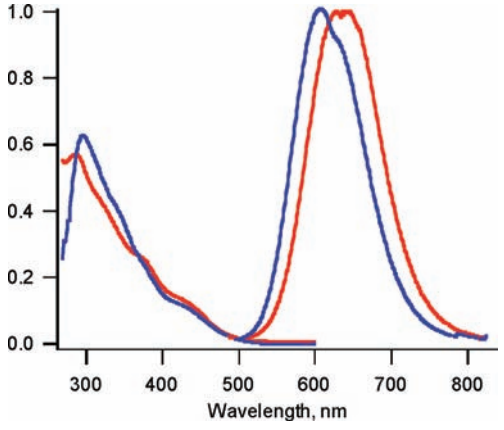

Figure 4. Absorption and emission spectra of **4** in THF (red) and benzene (blue).

and in each case, they are shorter in THF. In the series **1**− **4**, luminescence lifetimes decrease with decreasing emission energy. Lifetime values and the large Stokes' shifts suggest an excited state of triplet multiplicity. In benzene, the emission of each complex is slightly blue-shifted relative to that in THF.

As was observed for emission in the solid state and frozen glass, the order of emission energy in the series **1**−**4** (Figure 4) varies linearly with σ_p with the Hammett plot having a negative slope (Supporting Information, Figures S10−S11). This relationship supports the notion that substitution of the aryl amido group in the 4 position affects the energy of the highest occupied molecular orbital. Its energy level increases with the electron donating ability of the R^1 substituent.

In comparing the emission data in THF and benzene, emission energy, luminescence lifetime, and quantum yields are all lower in THF. These results suggest that the emissive excited state possesses charge transfer character which is stabilized better by the more polar solvent. The relationship between emission energy and lifetimes in the *same* solvent for **1**−**4** is possibly a manifestation of the "energy gap law" in which nonradiative decay pathways are more accessible to lower energy excited states.

In solution, the emission of **5** is slightly higher in energy than that of **6**. This differs from solid state and frozen glass measurements in which **6** exhibits higher energy emission. While the solid state and 77 K glass emission data suggest that the LUMO may be triazole-based, a higher energy LUMO in **6** is not supported in solution. A possible explanation is that conjugation of the triazole and phenyl ring in **5** differs between the fluid solution orientation and its average conformer in the solid state and frozen glass.[48]

dx.doi.org/10.1021/ic102338g |*Inorg. Chem.* 2011, 50, 3431–3441

Table 4. Electrochemical Potentials[a] (V versus NHE)[b,c]

complex	oxidation potential
1 Cu(**L1**)dppb	0.37[d]
2 Cu(**L2**)dppb	0.32[d]
3 Cu(**L3**)dppb	0.26[d]
4 Cu(**L4**)dppb	0.47[d]
5 Cu(**L5**)dppb	0.41 (0.15)[e]
6 Cu(**L6**)dppb	0.38 (0.16)[e]

[a] Measured in degassed THF with 0.1 M n-Bu_4NPF_6 as the supporting electrolyte using a glassy carbon working electrode with a Pt wire auxiliary electrode and Ag wire reference electrode. [b] Oxidation potentials obtained using ferrocene as an internal standard ($Fc^{+/0}$ = 0.56 V versus SCE in THF, SCE = 0.24 V versus NHE).[52] [c] The peak-to-peak difference for the ferrocene/ferrocenium$^+$ couple under these experimental conditions was 0.14 to 0.16 V. [d] Irreversible anodic wave. [e] Quasi-reversible oxidation with E_0 reported as $(E_{anodic} - E_{cathodic})/2$. Peak-to-peak difference value in parentheses.

Electrochemistry. Complexes **1**−**6** were studied by cyclic voltammetry in THF, and the results are shown in Table 4. Complexes **5** and **6** exhibit quasi-reversible oxidations at 0.41 and 0.38 V versus NHE, respectively. Conversely, **1**−**4** show irreversible oxidations at potentials ranging from 0.25 to 0.47 V versus NHE. No reduction waves were found within the solvent window. Facile oxidations are not surprising in view of the high oxygen sensitivity of the complexes in solution.

Oxidation potentials are an effective measure of the relative HOMO energies in a series of compounds. For **1**−**4**, the irreversible oxidation peak potential varies linearly with the σ_p parameter (Supporting Information, Figure S25), supporting the inferences made previously regarding the effect of R^1 on the photophysical properties. Complex **3**, with an electron-donating OMe group, is the most easily oxidized, while chloro-substituted **4** is the most difficult to oxidize. The nearly identical oxidation potentials determined for complexes **5** and **6** suggest that the N3 substituted triazole ring is not involved in the HOMO. Thus, the electrochemical data are consistent with an oxidation involving a portion of the molecule electronically coupled to the 4 position of the aryl amido ligand. The HOMO must be amido ligand-based or Cu(I)-based.

Complex **5** differs from **1** primarily by the 2,6-dimethyl substitution of the amido ligand. In the X-ray structure, the aryl substituent bound to the amido donor is twisted perpendicular to the triazole ring so that the methyl groups are located above and below the copper(I) ion. It is well-known that metal-to-ligand charge transfer in copper(I) complexes entails a formal oxidation from Cu(I) to Cu(II) and a possible geometrical change from tetrahedral toward square planar in the excited state.[49,50] As a result, addition of a ligand (solvent) is more likely to occur in the excited state, and oxidations may be irreversible during the electrochemical measurement. Complexes with bulky substituents near the Cu(I) ion are less prone to solvent coordination in the excited state.[51] In complexes **5** and **6**, the methyl groups of the amido ligand likely shield the metal center from coordination by THF upon electrochemical oxidation and allow some reversibility.

Electronic Structure Calculations. Density functional theory (DFT) calculations were performed on the singlet ground states (S_0) of complexes **1**−**6** to further probe the nature of the excited states and to clarify the discrepancies between emission energies in **5** and **6**. While the optimized geometry around the Cu(I) ions remains similar to that determined from the X-ray structure

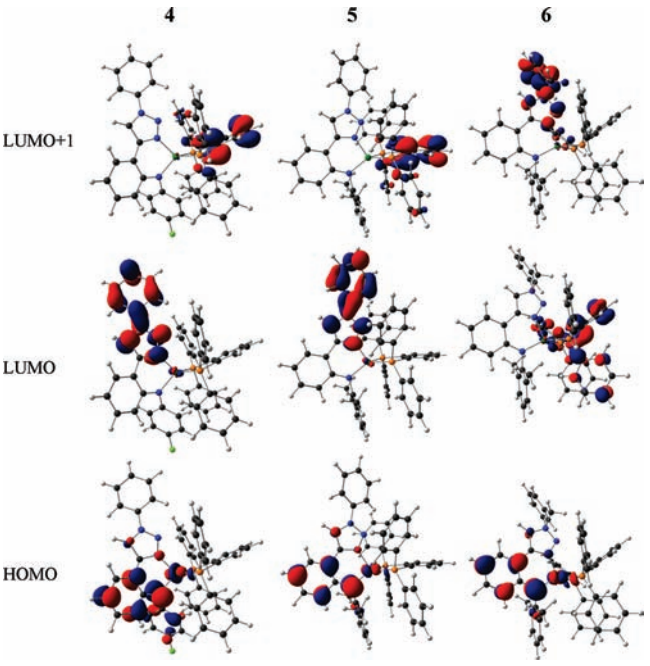

Figure 5. Frontier molecular orbitals for complexes **4**−**6** calculated at BP86/6-31G(d) level of theory.

Table 5. Frontier Orbital Energies for the Ground State of **1**−**6** in eV

complex	1	2	3	4	5	6
LUMO+1	−1.71	−1.73	−1.71	−1.81	−1.78	−1.56
LUMO	−2.13	−2.09	−2.12	−2.17	−1.90	−1.73
HOMO	−3.15	−3.11	−3.05	−3.26	−3.14	−3.11

determinations, significant differences are noted in the phenylene-N-(4-X aryl) torsion angles. The calculated torsion angles are 60.6° for **1**, 58.6° for **2**, 66.2° for **3**, and 56.4° for **4**. For 2,6-dimethyl substituted **5** and **6**, the substituted ring remains perpendicular to the phenylene ring. Dihedral angles between the triazole heterocycle and the N3 phenyl rings deviate slightly from planarity in the optimized geometry and lie in the range of 24.71° to 27.75°.

Diagrams of the HOMO, LUMO, and LUMO+1 for the ground states of **4**−**6** are shown in Figure 5, and energies of these orbitals for all complexes are provided in Table 5. Orbitals for complex **4** were chosen as a representative example for the series **1**−**4**. Complete diagrams for all complexes are provided in the Supporting Information. In all complexes, the HOMO is composed primarily of π-functions on the aryl amido ligand and d orbitals of the Cu(I) ion. In **1**−**4**, where the 4-substituted ring is *not* perpendicular to the phenylene ring, there are small contributions from π orbitals on the substituted ring to the HOMO. On the other hand, the perpendicularly oriented dimethyl substituted rings in **5** and **6** show negligible contributions to the HOMO. The electronic effect of the 4-substituted groups in **1**−**4** is evident in the energy level diagram. Complex **3** (σ_p = −0.28) has the highest HOMO level, while **4**, with the most electron-withdrawing substituent (σ_p = 0.24), possesses the lowest energy HOMO.

For complexes **1**−**5** with N3-phenyl triazole rings, the LUMO is delocalized over both rings. For **1**−**4**, there are only minor

dx.doi.org/10.1021/ic102338g |*Inorg. Chem.* 2011, 50, 3431–3441

deviations in the LUMO energies. The LUMO+1 level in **1**−**5** is composed of π-functions on the diphosphine ligand with the greatest contribution from the central dppb phenylene ring. In **6**, the LUMO is located on the dppb ligand and is nearly identical in character and energy to the LUMO+1 of **1**−**5** while the LUMO+1 level of **6** is composed of triazole and benzyl π functions despite the nonconjugating methylene group separating the two rings. In the absence of conjugation, the energy of this orbital (−1.56 eV) is greater than that of the corresponding conjugated triazole orbital in **5** (−1.90 eV).

Analyzed in the context of emission and electrochemical data, the electronic structure calculations provide valuable insight into the excited states. First, the optimized geometries suggest that free rotation of the 4-substituted N-aryl rings in **1**−**4** is possible, but rotation in **5** and **6** is hindered by the methyl groups. Rotation allows for conjugation between the amido donor and the phenylene backbone, and prevents electronic isolation of the *para* substituent. This is evident in the calculated HOMO energies, and experimentally in the oxidation potential, electronic spectra, and emission spectra which all vary according to the electronic influence of the *para* substituent.

While spectroscopy and electrochemistry shed light on the identity of the HOMO, the nature of the LUMO is not as easily ascertained experimentally. In the solid state and frozen glass samples, N-phenyl substituted **5** exhibited lower energy emission than N-benzyl substituted **6**, suggesting a triazole-based LUMO. Conversely, in solution the emission of **5** is higher energy than in **6**. DFT calculations provided insight into this discrepancy, showing that the LUMO of **5** is triazole-based, whereas the LUMO of **6** is actually diphosphine-based. In the absence of triazole conjugation for complex **6**, the triazole-based orbital energy is raised to the LUMO+1 level. The dissimilar nature of excited states in **5** and **6** helps to explain the additional low energy absorption feature in **6** as well as differences in lifetime data among **1**−**5** compared with **6**.

CONCLUSIONS

In pursuit of new photoluminescent Cu(I) compounds for application in OLEDs, we have prepared a series of mononuclear copper(I) complexes supported by 1,2-bis(diphenylphosphino) benzene and anionic amido-triazole ligands and investigated their structural, electrochemical, and photophysical properties. The complexes exhibit modest solution emission and bright solid state emission. Modification of the electronic properties of the amido ligand has led to elucidation of the HOMO as a mixture of Cu-d orbitals and biaryl amido π-functions. The LUMO, on the other hand, depends on the nature of the triazole ligand. For **1**−**5** in which the triazole is N3-phenyl substituted, the LUMO is located on the triazole and the emission is assigned as mixed metal-to-ligand + intraligand charge transfer ^{3}(MLCT+ILCT). A variation in ligand as simple as changing the N3-phenyl group to a benzyl group (complex **6**) results in a phosphine based LUMO and changes the assignment of the excited state to metal-to-ligand + ligand-to-ligand charge transfer ^{3}(MLCT+LLCT). While these complexes exhibit the desired photoluminescence and quasi-reversible electrochemistry desired for OLED devices, thermal decomposition remains a problem and sublimation is not feasible for vapor phase deposition processing. Nevertheless, these complexes are an important addition to the rapidly expanding literature on triazole coordination chemistry, and with judicious modification of the ligands, sublimation and device fabrication may be possible. Such efforts are currently underway.

EXPERIMENTAL SECTION

Chemicals. Trimethylsilylacetylene and 1-bromo-2-iodobenzene were purchased from Oakwood Chemicals. Substituted anilines, benzyl bromide, sodium azide, sodium *tert*-butoxide, and potassium *tert*-butoxide were purchased from Aldrich Chemical Co. and used as received. Palladium(II) acetate was purchased from Strem Chemicals. 1,1′-Bis-(diphenylphosphino)ferrocene was purchased from VWR. Toluene, THF, hexanes, and benzene were dried using a Grubbs-type solvent system and stored in a nitrogen-filled glovebox. 2-Methyltetrahydrofuran was distilled from sodium/benzophenone. Phenyl azide was prepared from aniline.

Characterization. ^{1}H, ^{13}C{^{1}H}, and ^{31}P{^{1}H} NMR spectra were recorded using a Bruker Avance 500 MHz spectrometer with ^{1}H and ^{13}C chemical shifts referenced to the residual solvent peaks in $CDCl_3$ or C_6D_6 and ^{31}P chemical shifts referenced to external 85% H_3PO_4. Mass spectra of the ligands and complexes were measured on a Shimadzu 2010 series liquid chromatography mass spectrometer (LCMS) under atmospheric pressure chemical ionization (APCI). Absorptions spectra were measured on a Hitachi U2000 UV−vis spectrometer. Steady-state excitation and emission spectra were obtained using a Spex Fluoromax-P fluorometer with excitation and emission slits set for a 2 nm bandpass. Solution phase samples were prepared using dry, deoxygenated benzene in a nitrogen-filled glovebox. Frozen glass samples were prepared in 5 mm NMR tubes in the glovebox and sealed with a septum. Solid state emission samples were measured as a finally ground mixture of the emissive complex and KBr (1:9 w/w) in a flame-sealed capillary tube. For low temperature measurements, the capillary was held in a vacuum dewar filled with liquid nitrogen. Lifetime measurements were performed using a model LN203C nitrogen laser (Laser Photonics Inc.) with λ = 337.1 nm and a 0.1 nm spectral width pulsed at 1 pulse/second. Signals were detected by a silicon photodiode and photomultiplier tube (1P28 type) with a 2 ns rise time and viewed with a Hewlett-Packard 54510-B oscilloscope connected to a computer via a GPIB interface. No less than five decay curves were averaged for data fitting. Elemental analyses were performed on a PerkinElmer 2400 Series II analyzer operated by the Center for Enabling New Technologies through Catalysis elemental analysis facility at the University of Rochester.

Electrochemistry. Cyclic voltammograms were measured using an EG&G PAR 263A potentiostat/galvanostat equipped with a single compartment cell using a glassy carbon working electrode, Ag wire pseudoreference electrode, and Pt wire auxiliary electrode. In all cases, a solution of tetrabutylammonium hexafluorophosphate (Fluka) in dry THF was purged with N_2 for 8 min, and a blank scan was obtained to verify the purity of the solvent. During purge, portions of solid copper(I) complex and ferrocene were added to the solution for measurements to obtain a concentration of about 1 mM complex. The scan rate was 100 mV s^{-1}.

Crystal Structure Determination. Each crystal was placed onto the tip of a glass fiber and mounted on a Bruker SMART Platform diffractometer equipped with an APEX II CCD area detector. All data were collected at 100.0(1) K using MoKα radiation (graphite monochromator.)[53] For each sample a preliminary set of cell constants and an orientation matrix were determined from reflections harvested from three orthogonal wedges of reciprocal space. Full data collections were carried out with frame exposure times of 45−60 s at detector distances of 4 cm. Randomly oriented regions of reciprocal space were surveyed for each sample: four major sections of frames were collected with 0.50° steps in ω at four different φ settings and a detector position of −38° in 2θ. The intensity data were corrected for absorption,[54] and final cell constants were calculated from the *xyz* centroids of approximately 4000 strong reflections from the actual data collection after integration.[53] Structures were solved using SIR97[55] and refined using SHELXL-97.[56]

dx.doi.org/10.1021/ic102338g |*Inorg. Chem.* 2011, 50, 3431–3441

Space groups were determined based on systematic absences, intensity statistics, and Cambridge Structural Database frequencies.[57] Direct-methods solutions were calculated which provided most non-hydrogen atoms from the difference Fourier map. Remaining non-hydrogen atoms were located through full-matrix least-squares (on F^2)/difference Fourier cycles. Non-hydrogen atoms were refined with anisotropic displacement parameters and hydrogen atoms were placed in ideal positions and refined as riding atoms with relative isotropic displacement parameters. All refinements were run to mathematical convergence.

DFT Calculations. The geometries obtained from X-ray crystallography were used as a starting point for geometry optimization in complexes **4**, **5**, and **6**. For **1**−**3**, the starting geometry of **4** was used. Ground state optimizations were first carried out at the HF/6-31G level in Gaussian 03. The resultant coordinates were input for optimization and single point calculations using the BP86 method which incorporates Becke's 1988 exchange functional[58] and Perdew's gradient corrections and correlation function[59] with the 6-31G(d) basis set on all atoms.

1-(Trimethylsilyl-ethynyl)-2-bromo-benzene. A solution of 1-iodo-2-bromobenzene (13.8 g) in diisopropyl amine (250 mL) was purged with a rapid flow of N_2 for 20 min. In one portion, CuI (0.33 g, 3.5%) and $Pd(PPh_3)_2Cl_2$ (0.34 g, 1%) were added. After stirring for 10 min, trimethylsilyl-acetylene (8.23 mL, 1.2 equiv) was added via syringe. A heavy precipitate formed immediately, and the mixture was stirred rapidly at room temperature for 5 h. The precipitate was removed via filtration, and the volatiles were evaporated leaving a black residue which was purified via flash chromatography on silica gel using hexanes as the eluent to provide 11.76 g of the title compound as a pale yellow oil (95% yield).

4-(2-Bromophenyl)-1-phenyl-1-*H*-1,2,3-triazole (C, R^2 = Ph). To a solution of **1** (4.24 g, 16.7 mmol) in 1:1 *t*BuOH/H_2O (50 mL) was added K_2CO_3 (5.6 g, 2 equiv). After stirring for 10 min, phenyl azide (2.00 g) and sodium ascorbate (0.20 g, 6%) were added. The mixture was purged with N_2 for 15 min then $CuSO_4$ (1.00 mL of a 0.5 M aqueous solution, 3%) was added dropwise with vigorous stirring. The reaction was stirred at room temperature for 1 h then at 60 °C for 24 h. Upon cooling, 50 mL of a dilute aqueous ammonia solution was added to provide a fine suspension which was extracted with diethyl ether. The ether layer was washed with brine, dried over $MgSO_4$ and evaporated. The residue was purified via flash column chromatography (silica gel, hexanes: ethyl acetate 10:1) to provide 2.97 g (59%) of the title compound a white powder. ^{1}H NMR ($CDCl_3$) δ 8.67 (s, 1H, triazole C-*H*), 8.20 (d, J = 7.7 Hz, 1H), 7.81 (d, J = 8.0 Hz, 2H), 7.69 (d, J = 8.0 Hz, 1H), 7.56 (t, J = 7.7 Hz, 2H), 7.45 (m, 2H), 7.24 (t, J = 7.7 Hz, 1H). MS (APCI+) m/z calcd. 299.01, 301.00. Found: 300.05, 302.05 $(M+H)^+$.

1-Benzyl-4-(2-bromophenyl)-1-*H*-1,2,3-triazole (C, R^2 = Bn). To a solution of **1** (1.00 g, 4 mmol) in 1:1 tBuOH/H_2O (15 mL) were added consecutively K_2CO_3 (1.1 g, 8 mmol), NaN_3 (0.28 g, 4.4 mmol), benzyl bromide (0.47 mL, 4 mmol), and sodium ascorbate (0.078 g, 0.4 mmol). The mixture was purged with N_2, and $CuSO_4$ (5%, 0.4 mL of a 0.5 M solution in water) was added via syringe. The reaction was heated at 65 °C for 24 h. Upon cooling, the mixture was diluted with aqueous ammonia and extracted with several portions of diethyl ether. The combined organic phase was washed with brine, dried ($MgSO_4$), and evaporated to give provide 0.90 g (73%) of the title compound as a pale yellow powder. ^{1}H NMR ($CDCl_3$, 500 MHz) δ 8.15 (s, 1H), 8.12 (d, J = 7.8 Hz, 1H), 7.63 (d, J = 8.0 Hz, 1H), 7.41−7.31 (m, 6H), 7.32−7.31 (m, 2H), 7.19 (dt, J = 7.7 Hz, 0.8 Hz, 1H), 5.61 (s, 2H). MS (APCI+) m/z calcd. 313.02, 315.02. Found: 313.95, 315.95 $(M+H)^+$.

Aryl Amination General Procedure. In a drybox, a Schlenk tube was charged with bromophenyl-triazole **C**, $Pd(OAc)_2$ (5%), 1,1′-bis-(diphenylphosphino)-ferrocene (dppf, 7.5%), sodium *tert*-butoxide (1.3 equiv.), and toluene (~3 mL/mmol). After stirring for 5 min, the appropriate aniline was added as a solid or as a solution in toluene. The flask was sealed with a Teflon stopper and heated at 100 °C for 48 h. Unless specified otherwise, the following workup procedure was used. After cooling the reaction, water was added. The aqueous layer was extracted with CH_2Cl_2, and the combined organic layers were washed with brine. After evaporation of the solvent, the crude products were adsorbed onto silica gel and the ligands were purified by column chromatography (hexanes:ethyl acetate 5:1).

***N*-Phenyl-2-(1-phenyl-1*H*-1,2,3-triazol-4-yl)aniline (HL1).** The general method was followed using bromo-phenyl triazole, **C** (1.00 g, 3.3 mmol), aniline (0.34 g, 3.7 mmol), $Pd(OAc)_2$ (37 mg), dppf (138 mg), and NaOtBu (0.416 g). After chromatography, the residue was triturated with pentane, filtered, and recrystallized from hot ethanol to provide white crystals. (0.85 g, 82%). ^{1}H NMR ($CDCl_3$, 500 MHz): δ 8.23 (s, 1H, triazole C*H*), 7.81−7.78 (m, 2H), 7.59−7.55 (m, 4H), 7.48 (tt, 2H, J = 1.2, 8.1), 7.32−7.22 (m, 5H), 6.98 (tt, 1H, J = 1.2, 7.1) 6.92 (dt, 1H, J = 1.1, 7.5). ^{13}C{^{1}H} NMR ($CDCl_3$, 125 MHz): δ 148.6 (q), 142.6 (q), 142.0 (q), 137.0 (q), 129.9, 129.4, 129.2, 129.1, 128.5, 121.9, 120.8, 119.7, 118.6, 116.9, 116.6 (q). MS (APCI+) m/z calcd. 312.14. Found: 313.05 $(M+H)^+$.

***N*-(4-Methylphenyl)-2-(1-phenyl-1*H*-1,2,3-triazol-4-yl)-aniline (HL2).** The general method was followed using bromo-phenyl triazole, **C** (1.00 g, 3.3 mmol), 4-toluidine (0.393 g, 3.7 mmol), $Pd(OAc)_2$ (37 mg), dppf (138 mg), and NaOtBu (0.416 g). After chromatography, the residue was triturated with hexanes, filtered, and recrystallized from hot ethanol to provide the title compound as white crystals (0.62 g, 57%). ^{1}H NMR ($CDCl_3$, 500 MHz): δ 8.23 (s, 1H, triazole C*H*), 7.80−7.79 (m, 2H), 7.58−7.55 (m, 3H), 7.48 (tt, 1H, J = 1.4, 7.4), 7.38 (dd, 1H, J = 0.8, 8.4), 7.23−7.12 (m, 5H), 6.88 (dt, 1H, J = 1.1, 7.4), 2.32 (s, 3H, CH_3). ^{13}C{^{1}H} NMR ($CDCl_3$, 125 MHz) δ 148.8 (q), 142.8 (q), 139.8 (q), 137.0 (q), 131.9 (q), 129.95, 129.94, 129.3, 129.1, 128.4, 121.1, 120.8, 119.0, 118.5, 116.0, 115.8 (q), 20.9 (−*C*H$_3$). MS (APCI+) m/z calcd. 326.15. Found: 327.30 $(M+H)^+$.

***N*-(4-Methoxyphenyl)-2-(1-phenyl-1*H*-1,2,3-triazol-4-yl)-aniline (HL3).** The general method was followed using bromo-phenyl triazole **C** (1.00 g, 3.3 mmol), 4-anisidine (0.452 g, 3.7 mmol), $Pd(OAc)_2$ (37 mg), dppf (138 mg), and NaOtBu (0.416 g). After chromatography, the residue was triturated with pentane, filtered, and recrystallized from hot ethanol to provide the title compound as white crystals (0.97 g, 85%). ^{1}H NMR ($CDCl_3$, 500 MHz): δ 8.25 (s, 1H, triazole C*H*), 7.81−7.80 (m, 2H), 7.57−7.47 (m, 4H), 7.49 (tt, 1H, J = 1.5, 7.5), 7.26−7.18 (m, 4H), 6.90 (d, 1H, J = 8.9), 6.85 (t, 1H, J = 7.2), 3.82 (s, 3H, CH_3). ^{13}C{^{1}H} NMR ($CDCl_3$, 125 MHz): δ 155.9 (q), 149.0 (q), 143.9 (q), 137.0 (q), 135.1 (q), 129.9, 129.3, 129.1, 128.3, 124.2, 120.8, 118.4, 118.3, 115.0, 114.8 (q), 114.7, 55.65 (-O*C*H$_3$). MS (APCI+) m/z calcd. 342.15. Found: 343.10 $(M+H)^+$.

***N*-(4-Chlorophenyl)-2-(1-phenyl-1*H*-1,2,3-triazol-4-yl)aniline (HL4).** The general method was followed using bromo-phenyl triazole **C** (1.00 g, 3.3 mmol), 4-chloroaniline (0.467 g, 3.7 mmol), $Pd(OAc)_2$ (37 mg), dppf (138 mg), and NaOtBu (0.416 g). After chromatography, the residue was triturated with hexanes, filtered, and recrystallized from hot ethanol to provide the product as white crystals (0.95 g, 85%). ^{1}H NMR ($CDCl_3$, 500 MHz): δ 8.23 (s, 1H, triazole C*H*), 7.80−7.79 (m, 2H), 7.59−7.56 (m, 3H), 7.49 (tt, 1H, J = 1.1, 7.5), 7.26−7.23 (m, 4H), 7.19−7.16 (m, 2H). ^{13}C{^{1}H} NMR ($CDCl_3$, 125 MHz): δ 148.6 (q), 141.7 (q), 141.3 (q), 136.9 (q), 130.0, 129.33, 129.29, 129.21, 128.5, 126.4 (q), 121.1, 120.8, 119.9, 118.6, 116.7, 116.6 (q). MS (APCI+) m/z calcd. 346.10 Found: 347.05 $(M+H)^+$.

2,6-Dimethyl-*N*-[2-(1-phenyl-1*H*-1,2,3-triazol-4-yl)phenyl]-aniline (HL5). The general procedure for aryl amination was followed using **C** (0.500 g, 1.6 mmol), $Pd(OAc)_2$ (11 mg), dppf (41 mg), NaO*t*Bu (0.19 g), and 2,6-dimethylaniline (0.25 mL) in 10 mL of toluene. After chromatography, the residue was crystallized from a 1:5 mixture of acetonitrile/ethanol to provide **HL5** as white blocks upon standing at room temperature (244 mg, 43%). ^{1}H NMR ($CDCl_3$, 400 MHz): δ 8.86 (s, 1H, NH), 8.23 (s, 1H, triazole C*H*), 7.83 (d, 2H, J = 7.6), 7.60−7.47 (m, 4H), 7.16−7.07 (m, 4H), 6.74 (t, 1H, J = 7.4), 6.31 (d, 1H,

J = 8.4), 2.27 (s, 6H, $-CH_3$). $^{13}C\{^1H\}$ NMR ($CDCl_3$, 125 MHz): δ 149.6 (q), 144.9 (q), 138.6 (q), 137.1 (q), 136.7 (q), 130.0, 129.6, 129.1, 128.5, 128.0, 126.0, 120.8, 118.0, 116.8, 113.0 (q), 112.9, 18.6 ($-CH_3$). MS (APCI+) m/z calcd. 370.17 Found: 341.15 $(M+H)^+$.

2,6-Dimethyl-*N*-[2-(1-benzyl-1*H*-1,2,3-triazol-4-yl)phenyl]-aniline (HL6). The general procedure was followed using **C** (2.00 g, 6.4 mmol), $Pd(OAc)_2$ (43 mg), sodium *tert*-butoxide (0.73 g), dppf (0.159 g), toluene (15 mL), and 2,6-dimethylaniline (0.87 mL). Upon completion, the reaction was cooled, and 50 mL of water was added. The aqueous layer was extracted with diethyl ether (3 × 100 mL). Ether was removed under reduced pressure, and the residue was triturated with a small amount of ethanol which was then decanted from the tan solid. Crystallization of the solid from hot EtOH provided the title compound as white needles (1.36 g, 60.3%). ^1H NMR ($CDCl_3$, 400 MHz) δ 8.94 (s, 1H, N−H), 7.76 (s, 1H), 7.42−7.34 (m, 6H), 7.15−7.09 (m, 3H), 7.03 (t, J = 7.2 Hz, 1H), 6.66 (t, J = 7.4 Hz, 1H), 6.27 (d, J = 8.2 Hz, 1H), 5.61 (s, 2H, CH_2), 2.24 (s, 6H, CH_3). $^{13}C\{H\}$ NMR ($CDCl_3$, 125 MHz): δ 149.4 (q), 144.7 (q), 138.6 (q), 136.7 (q), 134.6 (q), 129.3, 129.2, 129.0, 128.5, 128.3, 127.8, 125.9, 119.8, 116.5, 113.1 (q), 112.8, 54.6 ($-CH_2$-), 18.6 ($-CH_3$). MS (APCI+) m/z calcd. 354.18. Found: 355.15 $(M+H)^+$.

General Procedure for Cu(amido-triazole)dppb Complex Synthesis. To a solution of ligand precursor in THF was added solid potassium *tert*-butoxide. After agitation, this solution was dropwise added to a stirred slurry of $[CuCl(dppb)]_2$ in THF. The reaction was stirred with moderate warming (<40 °C) until nearly clear and then filtered through celite to remove KCl. The solution was concentrated to 1−2 mL, and hexanes were added slowly to precipitate the product which was collected by filtration, washed with hexanes, and dried under vacuum.

Cu(L1)(dppb) (1). The general procedure was followed using 0.050 g of **HL1**, 0.020 g of *t*BuOK, and 0.080 g of $[dppbCuCl]_2$ to provide 0.102 g of **1** as a yellow powder (76% yield). ^1H NMR (C_6D_6, 500 MHz): 7.72 (dd, J = 2.3, 7.7 1H), 7.48−7.42 (m, 10H), 7.38−7.36 (m, 3H), 7.35 (s, 1H), 7.28 (dd, J = 1.8, 7.3, 1H), 7.24−7.21 (m, 2H), 7.03−6.90 (m, 20H), 6.77 (tt, J = 1.1 7.2, 1H), 6.24−6.59 (m, 1H), 6.90−6.82 (m, 2H), 6.61−6.58 (m, 1H), 2.23 (s, 3H). $^{31}P\{^1H\}$ NMR (C_6D_6, 202 MHz): δ −12.4. MS (APCI+) m/z calcd 820.19. Found: 821.50 $(M+H)^+$ Anal. Calcd. for $C_{50}H_{39}CuN_4P_2$: C, 73.11; H, 4.79; N, 6.82. Found: C, 73.06; H, 5.17; N, 6.31.

Cu(L2)(dppb) (2). The general procedure was followed using 0.053 g of **HL2**, 0.020 g of *t*BuOK, and 0.080 g of $[dppbCuCl]_2$ to provide 0.101 g of complex **2** as an orange powder (75%). ^1H NMR (C_6D_6, 500 MHz): 7.66 (dd, J = 1.0, 7.7 1H), 7.48−7.40 (m, 10H), 7.37 (s, 1H), 7.30 (dd, J = 1.7, 7.3, 1H), 7.25−7.22 (m, 3H), 7.02−6.91 (m, 19H), 6.90−6.82 (m, 2H), 6.61−6.58 (m, 1H), 2.23 (s, 3H). $^{31}P\{^1H\}$ NMR-(C_6D_6, 202 MHz): δ −12.4. MS (APCI+) m/z calcd 834.21. Found: 835.30 $(M+H)^+$ Anal. Calcd. for $C_{51}H_{41}CuN_4P_2$: C, 73.33; H, 4.95; N, 6.71. Found: C, 73.88; H, 5.00; N, 6.32.

Cu(L3)(dppb) (3). The general procedure was followed using 0.052 g of **L3**, 0.020 g of *t*BuOK, and 0.080 g of $[dppbCuCl]_2$ to provide 0.112 g of **3** as an orange powder (84%). ^1H NMR (C_6D_6, 500 MHz): 7.54−7.53 (d, J = 8.6, 1H), 7.47−7.38 (m, 10H), 7.33 (s, 1H), 7.32−7.30 (m, 2H), 7.27−7.24 (m, 1H), 7.02−6.84 (m, 20H), 6.65−6.64 (m, 2H), 6.60−6.57 (m, 1H), 3.44 (s, 3H). $^{31}P\{^1H\}$ NMR(C_6D_6, 202 MHz): δ −12.1. MS (APCI+) m/z calcd 850.21. Found: 851.40 $(M+H)^+$ Anal. Calcd. for $C_{51}H_{41}CuN_4OP_2$: C, 71.95; H, 4.85; N, 6.58. Found: C, 71.80; H, 4.89; N, 6.34.

Cu(L4)(dppb) (4). The general procedure was followed using 0.056 g of **HL4**, 0.020 g of *t*BuOK, and 0.180 g of $[dppbCuCl]_2$ to provide 0.096 g of complex **4** as an orange powder (70%). X-ray quality crystals were obtained from a mixture of precipitate and filtrate which was left to stand prior to filtration. ^1H NMR (C_6D_6, 500 MHz): 7.61−7.59 (m, 1H), 7.56−7.41 (m, 10H), 7.31 (s, 1H), 7.24−7.18 (m, 4H), 7.07−7.01 (m, 2H), 7.01−6.86 (m, 19H), 6.61 (t, 1H, J = 7.3). $^{31}P\{^1H\}$ NMR(C_6D_6, 202 MHz): δ −10.7. MS (APCI+) m/z calcd. 854.16. Found: 855.10 $(M+H)^+$ Anal. Calcd. for $C_{50}H_{39}ClCuN_4P_2$: C, 70.17; H, 4.48; N, 6.55. Found: C, 69.79; H, 4.70; N, 6.40

Cu(L5)(dppb) (5). The general procedure was followed using 0.164 g of **HL5**, 0.065 g of *t*BuOK, and 0.263 g of $[dppbCuCl]_2$ to provide 0.390 g of **5** as an orange powder (95%). X-ray quality crystals were obtained from a mixture of precipitate and filtrate which was left to stand prior to filtration. ^1H NMR (C_6D_6, 500 MHz): δ 7.46−7.41 (m, 4H), 7.34 (s, 1H), 7.33−7.32 (m, 2H), 7.28−7.27 (m, 2H), 7.12−7.09 (m, 3H), 7.04−6.95 (m, 3H), 6.97−6.82 (m, 20H), 6.70 (dd, J = 1.1, 6.7, 1H), 6.49 (m, 1H), 2.44 (s, 6H, CH_3). $^{31}P\{^1H\}$ NMR (C_6D_6, 202 MHz): δ −10.4. MS (APCI+) m/z calcd. 848.23. Found: 849.40 $(M+H)^+$ Anal. Calcd. for $C_{52}H_{43}CuN_4P_2$: C, 73.53; H, 5.10; N, 6.60. Found: C, 73.50; H, 5.13; N, 6.42.

Cu(L6)(dppb) (6). The general procedure was followed using 0.244 g of **HL6**, 0.077 g of *t*BuOK, and 0.333 g of $[dppbCuCl]_2$ to provide 0.486 g of **6** as a yellow powder (92%). X-ray quality crystals were obtained from slow evaporation of the filtrate after filtration of the bulk product or by vapor diffusion of hexanes into THF. ^1H NMR (C_6D_6, 500 MHz): δ 7.46−7.41 (m, 3H), 7.28−7.26 (m, 3H), 7.16−7.12 (m, 2H), 7.07−6.80 (m, 25H), 6.69−6.65 (m, 3H), 6.39−6.36 (m, 1H), 4.48 (s, 2H, CH_2), 2.43 (s, 6H, CH_3). $^{31}P\{^1H\}$ NMR(C_6D_6, 202 MHz): δ −12.4. MS (APCI+) m/z calcd. 862.24 Found: 862.95 $(M+H)^+$ Anal. Calcd. for $C_{53}H_{45}CuN_4P_2 \cdot$ THF (THF by ^1H NMR): C, 73.18; H, 5.71; N, 5.99. Found: C, 73.49; H, 5.94; N, 6.04.

■ ASSOCIATED CONTENT

Supporting Information. Crystallographic data in CIF format. Further details are given in Figures S1−S27 and Tables S1−S6. This material is available free of charge via the Internet at http://pubs.acs.org.

■ ACKNOWLEDGMENT

We thank the National Science Foundation GOALI program (Grant CHE-0616782) for support of this research.

■ AUTHOR INFORMATION

Corresponding Author
*E-mail: eisenberg@chem.rochester.edu.

■ REFERENCES

(1) *Transition Metal and Rare Earth Compounds III*; Yersin, H., Ed.; Springer: Berlin, 2004; Vol. 241, p 1.
(2) Moudam, O.; Kaeser, A.; Delavaux-Nicot, A.; Duhayon, C.; Holler, M.; Accorsi, G.; Armaroli, N.; Seguy, I.; Navarro, J.; Destruel, P.; Nierengarten, J. F. *Chem. Commun.* **2007**, 3077.
(3) Tsuboyama, A.; Kuge, K.; Furugori, M.; Okada, S.; Hoshino, M.; Ueno, K. *Inorg. Chem.* **2007**, *46*, 1992.
(4) Su, Z. S.; Che, G. B.; Li, W. L.; Su, W. M.; Li, M. T.; Chu, B.; Li, B.; Zhang, Z. Q.; Hu, Z. Z. *Appl. Phys. Lett.* **2006**, 88.
(5) Che, G. B.; Su, Z. S.; Li, W. L.; Chu, B.; Li, M. T.; Hu, Z. Z.; Zhang, Z. Q. *Appl. Phys. Lett.* **2006**, 89.
(6) Si, Z. J.; Li, J.; Li, B.; Liu, S. Y.; Li, W. L. *J. Lumin.* **2009**, *129*, 181.
(7) Zhang, L. M.; Li, B. *J. Electrochem. Soc.* **2009**, *156*, J174.
(8) Zhang, L. M.; Li, B.; Su, Z. M. *J. Phys. Chem. C.* **2009**, *113*, 13968.
(9) Zhang, Q. S.; Ding, J. Q.; Cheng, Y. X.; Wang, L. X.; Xie, Z. Y.; Jing, X. B.; Wang, F. S. *Adv. Funct. Mater.* **2007**, *17*, 2983.
(10) Armaroli, N.; Accorsi, G.; Holler, M.; Moudam, O.; Nierengarten, J. F.; Zhou, Z.; Wegh, R. T.; Welter, R. *Adv. Mater.* **2006**, *18*, 1313.
(11) Wang, Y. M.; Teng, F.; Hou, Y. B.; Xu, Z.; Wang, Y. S.; Fu, W. F. *Appl. Phys. Lett.* **2005**, 87.
(12) Harkins, S. B.; Peters, J. C. *J. Am. Chem. Soc.* **2005**, *127*, 2030.

(13) Deaton, J. C. K.; Denis, Y.; Young, Ralph, H.; Pawlik, Thomas, D.; Peters, Jonas, C.; Mickenberg, Seth, F.; Eisenberg, Richard, S. *Dig. Tech. Pap.-Soc. Inf. Disp. Int. Symp.* **2009**, *40*, 691.
(14) Deaton, J. C.; Switalski, S. C.; Kondakov, D. Y.; Young, R. H.; Pawlik, T. D.; Giesen, D. J.; Harkins, S. B.; Miller, A. J. M.; Mickenberg, S. F.; Peters, J. C. *J. Am. Chem. Soc.* **2010**, *132*, 9499.
(15) Rostovtsev, V. V.; Green, L. G.; Fokin, V. V.; Sharpless, K. B. *Angew. Chem., Int. Ed.* **2002**, *41*, 2596.
(16) Tornoe, C. W.; Christensen, C.; Meldal, M. *J. Org. Chem.* **2002**, *67*, 3057.
(17) Meldal, M.; Tornoe, C. W. *Chem. Rev.* **2008**, *108*, 2952.
(18) Struthers, H.; Mindt, T. L.; Schibli, R. *Dalton Trans.* **2010**, *39*, 675.
(19) Urankar, D.; Pinter, B.; Pevec, A.; De Proft, F.; Turel, I.; Kosmrlj, J. *Inorg. Chem.* **2010**, *49*, 4820.
(20) Hao, E. R.; Wang, Z. Y.; Jiao, L. J.; Wang, S. W. *Dalton Trans.* **2010**, *39*, 2660.
(21) Crowley, J. D.; Gavey, E. L. *Dalton Trans.* **2010**, *39*, 4035.
(22) Crowley, J. D.; Bandeen, P. H.; Hanton, L. R. *Polyhedron* **2010**, *29*, 70.
(23) Bai, S. Q.; Leelasubcharoen, S.; Chen, X.; Koh, L. L.; Zuo, J. L.; Hor, T. S. A. *Cryst. Growth Des.* **2010**, *10*, 1715.
(24) Schweinfurth, D.; Pattacini, R.; Strobel, S.; Sarkar, B. *Dalton Trans.* **2009**, 9291.
(25) van Assema, S. G. A.; Tazelaar, C. G. J.; de Jong, G. B.; van Maarseveen, J. H.; Schakel, M.; Lutz, M.; Spek, A. L.; Slootweg, J. C.; Lammertsma, K. *Organometallics* **2008**, *27*, 3210.
(26) Schweinfurth, D.; Hardcastle, K. I.; Bunz, U. H. F. *Chem. Commun.* **2008**, 2203.
(27) Richardson, C.; Fitchett, C. M.; Keene, R.; Steel, P. J. *Dalton Trans.* **2008**, 2534.
(28) Ohi, H.; Shimizu, M.; Obata, M.; Funabiki, T.; Yano, S. *Acta. Crystallogr., Sect. E* **2008**, *64*, M1256.
(29) Obata, M.; Kitamura, A.; Mori, A.; Kameyama, C.; Czaplewska, J. A.; Tanaka, R.; Kinoshita, I.; Kusumoto, T.; Hashimoto, H.; Harada, M.; Mikata, Y.; Funabiki, T.; Yano, S. *Dalton Trans.* **2008**, 3292.
(30) Fletcher, J. T.; Bumgarner, B. J.; Engels, N. D.; Skoglund, D. A. *Organometallics* **2008**, *27*, 5430.
(31) Badeche, S.; Daran, J. C.; Ruiz, J.; Astruc, D. *Inorg. Chem.* **2008**, *47*, 4903.
(32) Suijkerbuijk, B.; Aerts, B. N. H.; Dijkstra, H. P.; Lutz, M.; Spek, A. L.; van Koten, G.; Gebbink, R. *Dalton Trans.* **2007**, 1273.
(33) Li, Y. J.; Huffman, J. C.; Flood, A. H. *Chem. Commun.* **2007**, 2692.
(34) Detz, R. J.; Heras, S. A.; de Gelder, R.; van Leeuwen, P.; Hiemstra, H.; Reek, J. N. H.; van Maarseveen, J. H. *Org. Lett.* **2006**, *8*, 3227.
(35) Chan, T. R.; Hilgraf, R.; Sharpless, K. B.; Fokin, V. V. *Org. Lett.* **2004**, *6*, 2853.
(36) Donnelly, P. S.; Zanatta, S. D.; Zammit, S. C.; White, J. M.; Williams, S. J. *Chem. Commun.* **2008**, 2459.
(37) Ozcubukcu, S.; Ozkal, E.; Jimeno, C.; Pericas, M. A. *Org. Lett.* **2009**, *11*, 4680.
(38) Bergbreiter, D. E.; Hamilton, P. N.; Koshti, N. M. *J. Am. Chem. Soc.* **2007**, *129*, 10666.
(39) Manbeck, G. F.; Brennessel, W. W.; Evans, C. M.; Eisenberg, R. *Inorg. Chem.* **2010**, *49*, 2834.
(40) Bai, S. Q.; Kwang, J. Y.; Koh, L. L.; Young, D. J.; Hor, T. S. A. *Dalton Trans.* **2010**, *39*, 2631.
(41) Monkowius, U.; Ritter, S.; Konig, B.; Zabel, M.; Yersin, H. *Eur. J. Inorg. Chem.* **2007**, 4597.
(42) Xiang, J.; Yin, Y. G.; Mei, P. *Inorg. Chem. Commun.* **2007**, *10*, 1168.
(43) Miller, A. J. M.; Dempsey, J. L.; Peters, J. C. *Inorg. Chem.* **2007**, *46*, 7244.
(44) Driver, M. S.; Hartwig, J. F. *J. Am. Chem. Soc.* **1996**, *118*, 7217.
(45) Goj, L. A.; Blue, E. D.; Munro-Leighton, C.; Gunnoe, T. B.; Petersen, J. L. *Inorg. Chem.* **2005**, *44*, 8647.
(46) Moudam, O.; Kaeser, A.; Delavaux-Nicot, B.; Duhayon, C.; Holler, M.; Accorsi, G.; Armaroli, N.; Seguy, I.; Navarro, J.; Destruel, P.; Nierengarten, J. F. *Chem. Commun.* **2007**, 3077.
(47) Nakamaru, K. *Bull. Chem. Soc. Jpn.* **1982**, *55*, 2697.
(48) A reviewer suggested aggregation effects as a possible explanation. To test for this, emission spectra of **5** and **6** were recorded in THF at a range of concentrations and supplied as Supporting Information. While the intensity of emission is quenched at higher concentrations (1×10^{-3}), emission maxima are not concentration dependent in these compounds.
(49) Armaroli, N.; Accorsi, G.; Cardinali, F.; Listorti, A. In *Photochemistry and Photophysics of Coordination Compounds I*; Springer: Berlin, 2007; Vol. 280, p 69.
(50) Coppens, P.; Vorontsov, I. I.; Graber, T.; Kovalevsky, A. Y.; Chen, Y. S.; Wu, G.; Gembicky, M.; Novozhilova, I. V. *J. Am. Chem. Soc.* **2004**, *126*, 5980.
(51) Scaltrito, D. V.; Thompson, D. W.; O'Callaghan, J. A.; Meyer, G. J. *Coord. Chem. Rev.* **2000**, *208*, 243.
(52) Connelly, N. G.; Geiger, W. E. *Chem. Rev.* **1996**, *96*, 877.
(53) *SAINT*; Bruker AXS: Madison WI, 2008.
(54) *APEX2*; Bruker AXS: Madison, WI, 2009.
(55) Altomare, A. B.; Burla, M. C.; Camalli, M.; Cascarano, G. L.; Giacovazzo, C.; Guagliardi, A.; Moliterni, A. G. G.; Polidori, G.; Spagna, R. *SIR97*; Istituto di Cristallografio, CNR: Bari, Italy, 1999.
(56) Sheldrick, G. M. *Acta Crystallogr.* **2008**, *A64*, 112.
(57) Allen, F. *Acta Crystallogr.* **2002**, *B58*, 380.
(58) Becke, A. D. *Phys. Rev. A* **1988**, *38*, 3098.
(59) Perdew, J. P. *Phys. Rev. B.* **1986**, *33*, 8822.